Extratropical–Tropical Interaction Model Intercomparison Project (Etin-Mip): Protocol and Initial Results

Sarah M. Kang, Matt Hawcroft, Baoqiang Xiang, Yen-Ting Hwang, Gabriel Cazes, Francis Codron, Traute Crueger, Clara Deser, Oivind Hodnebrog, Hanjun Kim, et al.

EXTRATROPICAL–TROPICAL INTERACTION MODEL INTERCOMPARISON PROJECT (ETIN-MIP)

Protocol and Initial Results

Sarah M. Kang, Matt Hawcroft, Baoqiang Xiang, Yen-Ting Hwang, Gabriel Cazes, Francis Codron, Traute Crueger, Clara Deser, Øivind Hodnebrog, Hanjun Kim, Jiyeong Kim, Yu Kosaka, Teresa Losada, Carlos R. Mechoso, Gunnar Myhre, Øyvind Seland, Bjorn Stevens, Masahiro Watanabe, and Sungduk Yu

ETIN-MIP is a community-wide effort to improve dynamical understanding of the linkages between tropical precipitation and radiative biases in various regions, with implications for anthropogenic climate change and geoengineering.

The intertropical convergence zone (ITCZ) is a narrow equatorial band of intense rainfall that receives one-third of the global precipitation. Even a minor shift in the ITCZ position is of great societal relevance not only because billions of people depend on this water source for their freshwater and food production but also because the latent heat released by condensation of water vapor in the atmosphere associated with tropical precipitation drives profound global impacts via poleward propagating Rossby waves (Hoskins and Karoly 1981). Moreover, a displacement in the ITCZ position exerts a considerable influence on the extratropics through changes in the frequency of tropical cyclones (Dunstone et al. 2013; Merlis et al. 2013), the poleward edge of the Hadley circulation (Kang and Lu 2012; Chemke and Polvani 2019), and the midlatitude jet position (Ceppi et al. 2013; Cvijanovic et al. 2013). It is for these reasons that the question of what controls the position, strength, and variability of the tropical rainbelts has emerged as one of the central questions of climate science (Bony et al. 2015).

Despite the crucial importance of correctly simulating the distribution of tropical precipitation, generations of global climate models (GCMs) have had difficulty simulating the observed pattern of tropical precipitation, with a too-pronounced "double ITCZ" (Mechoso et al. 1995; Zhang et al. 2015) being a robust bias. Great effort has been made to correct this bias because it substantially influences the reliability of future climate projections (Zhou and Xie 2015). This bias manifests in both hemispherically symmetric and antisymmetric components (Adam et al. 2016): the symmetric component is characterized by deficient precipitation in the equatorial region and excessive precipitation in the off-equatorial region; the antisymmetric component is characterized by an overestimation of precipitation in the southern

tropics relative to the northern tropics manifested in a too zonally oriented and eastward extended South Pacific convergence zone (SPCZ). In this study, we will refer to the hemispherically antisymmetric component as the double ITCZ bias. In general, the double ITCZ bias has been attributed to local origins such as poor representation of tropical ocean–atmosphere feedbacks (Lin 2007), stratocumulus clouds (Ma et al. 1996) and associated bias in tropical radiative fluxes from atmospheric models (Xiang et al. 2017), unrealistic representation of convective entrainment rate (Hirota et al. 2011), biased sea surface temperature (SST) thresholds leading to the erroneous onset of deep convection (Bellucci et al. 2010), and unrealistic winds in the eastern Pacific and coastal areas (De Szoeke and Xie 2008; Zheng et al. 2011). In a recent paper, Song and Zhang (2018) report on a major reduction of the double ITCZ bias in their model with a revised parameterization of deep convection.

On the other hand, extratropical energy biases have also been proposed as a possible cause of the double ITCZ bias. In particular, the warm bias in the Southern Hemisphere extratropics, observed in many GCMs associated with cloud biases over the Southern Ocean, is suggested to contribute to the double ITCZ bias (Hwang and Frierson 2013; Li and Xie 2014). In response to the hemispheric energy imbalance associated with a warmer Southern Hemisphere, the Hadley circulation adjusts in a way to transport energy northward via its upper branch while transporting moisture southward via its lower branch (Kang et al. 2008), thereby potentially driving the double ITCZ. This energetics framework, which relates the ITCZ response to the energy transport by the Hadley circulation, has been successfully invoked in a number of studies to explain how the ITCZ responds to extratropical thermal forcing in global climate models that do not include ocean dynamics (e.g., Broccoli et al. 2006; Kang et al. 2009). Slab ocean coupled GCM experiments even suggest the extratropics as the forcing location most effective at shifting the ITCZ position (Seo et al. 2014), lending credibility to the hypothesis that remote effects of the Southern Ocean warm bias are major contributors to the double ITCZ bias.

To investigate this hypothesis, several recent studies perturbed the Southern Hemisphere extratropics in fully coupled atmosphere–ocean models. Kay et al. (2016) enhance cloud brightness over the Southern Ocean, which is shown to result in little shift in tropical precipitation, in contrast to the expectation based on slab ocean model studies. Similarly, Hawcroft et al. (2017) apply targeted albedo corrections in the Southern Ocean and the double ITCZ problem persists. Mechoso et al. (2016) artificially reduce insolation over the southern extratropics in two independent models. The one that more realistically simulates the sensitivity of stratocumulus to underlying SST shows some improvement in the double ITCZ bias, though only partially in the zonal mean. Xiang et al. (2018) contrast the tropical precipitation response to increased insolation over the southern extratropics and the southern tropics, respectively. While the southern tropical forcing is certainly more effective at shifting the ITCZ, the extent of the ITCZ shift in response to the southern extratropical forcing is still more significant than in other aforementioned studies. The same conclusion is drawn from the experiments where stratospheric aerosols that reflect incoming radiation are imposed in defined latitude

AFFILIATIONS: Kang, H. Kim, and J. Kim—School of Urban and Environmental Engineering, Ulsan National Institute of Science and Technology, Ulsan, South Korea; Hawcroft—University of Exeter, Exeter, United Kingdom, and University of Southern Queensland, Toowoomba, Queensland, Australia; Xiang—NOAA/Geophysical Fluid Dynamics Laboratory, Princeton, New Jersey, and University Corporation for Atmospheric Research, Boulder, Colorado; Hwang—Department of Atmospheric Sciences, National Taiwan University, Taipei, Taiwan; Cazes—School of Engineering, Universidad de la República, Montevideo, Uruguay; Codron—LOCEAN/IPSL, Sorbonne Université, CNRS, IRD, MNHN, Paris, France; Crueger and Stevens—Max Planck Institute for Meteorology, Hamburg, Germany; Deser—Climate and Global Dynamics, National Center for Atmospheric Research, Boulder, Colorado; Hodnebrog and Myhre—Center for International Climate Research (CICERO), Oslo, Norway; Kosaka—Research Center for Advanced Science and Technology, The University of Tokyo, Tokyo, Japan; Losada—Department of Earth Physics and Astrophysics, Faculty of Physics, Universidad Complutense de Madrid, Madrid, Spain; Mechoso—Department of Atmospheric and Oceanic Sciences, University of California, Los Angeles, Los Angeles, California; Seland—Norwegian Meteorological Institute, Oslo, Norway; Watanabe—Atmosphere and Ocean Research Institute, The University of Tokyo, Tokyo, Japan; Yu—Department of Geology and Geophysics, Yale University, New Haven, Connecticut

CORRESPONDING AUTHOR: Sarah M. Kang, skang@unist.ac.kr

The abstract for this article can be found in this issue, following the table of contents.

DOI:10.1175/BAMS-D-18-0301.1

A supplement to this article is available online (10.1175/BAMS-D-18-0301.2)

In final form 26 August 2019

bands (Hawcroft et al. 2018). In sum, the ITCZ shift responses to extratropical energy perturbations are only modest in dynamic ocean coupled GCMs, though with substantial differences among models.

The damped ITCZ response in fully coupled simulations relative to slab ocean simulations is because energy perturbations need not be balanced by the atmosphere alone but are also mediated by changes in oceanic heat transport. The less the energy perturbations are balanced by changes in atmospheric heat transport, due to oceanic compensation, the smaller the ITCZ shift response. Previous studies indicate a wide range of the atmospheric fractional contribution to the total cross-equatorial energy transport response to the Southern Hemisphere extratropical cooling that spans between 20% (Kay et al. 2016) and 62% (Hawcroft et al. 2018). Such differences may stem from differences in experimental design, different model physics, or underlying biases in any given model. To address this issue, Kang et al. (2018a) suggest that multimodel comparisons should be constructed to cleanly examine the nature and the spread of model response to prescribed energy perturbations at different latitude bands.

This proposal has resulted in the Extratropical–Tropical Interaction Model Intercomparison Project (ETIN-MIP). The Green's function approach would be ideal for thoroughly assessing the global impact of regional energy perturbations, and was adopted in either an AMIP-type prescribed SST setting (Zhou et al. 2017) or a slab ocean setting (F. Liu et al. 2018) where warming or cooling is added over a limited domain throughout the entire globe. However, this is prohibitive in practice for fully coupled models due to the high computational cost. As an alternative approach, ETIN-MIP proposes to selectively perturb three target regions of persistent model biases in fully coupled models. Previous studies have adopted a similar approach, but used one fully coupled climate model (e.g., Hawcroft et al. 2018; Xiang et al. 2018; White et al. 2018). ETIN-MIP will cast light on which regions are particularly important and sensitive to energy perturbations/biases in the context of their teleconnections and whether this sensitivity is robust by investigating causes of intermodel diversity and the specific processes that govern any spread in the models' response.

Numerical experiments defined by ETIN-MIP are guided by four core science questions:

- How sensitive is the partitioning of energy transport response between the atmosphere and ocean to the region of forcing?
- Does the ocean heat transport response primarily result from dynamic ocean circulation changes or ocean temperature anomalies?
- Which part of the ocean circulation (i.e., Ekman transport, subtropical gyres, deep overturning circulation) is most effective at inducing cross-equatorial energy transport?
- How much does the intermodel response spread vary with forcing location and what are the implications for understanding (i) the causes of bias in the climatology of those models and (ii) the likely fidelity of their future projections, individually and collectively?

By answering these questions, ETIN-MIP aims to provide an improved understanding of the link between tropical precipitation and regional energy anomalies that are both local and remote. Moreover, ETIN-MIP will provide a platform to study the causes of climatological biases in coupled models at a process level, and the plausibility of model responses to external perturbations, thereby contributing to improve our ability to make robust future projections of regional patterns of climate change.

EXPERIMENTAL DESIGN. The first tier of ETIN-MIP asks modeling groups to perform one control and three perturbation experiments with their state-of-the-art fully coupled models. The control experiment (CNTL) is a fully spun-up preindustrial run where 150 simulated years of output is requested to be provided from a start date chosen to initialize subsequent perturbation experiments. The three perturbation experiments are also integrated for 150 years after an abrupt reduction of solar flux over three different latitude bands: the southern extratropics between 45° and 65°S (SEXT), the southern tropics between 5° and 25°S (STRO), and the northern extratropics between 45° and 65°N (NEXT). The geographical distribution of solar flux perturbations in all experiments are shown in Fig. 1. The forcing domains correspond to regions with the largest intermodel spread in cloud radiative effects (Boucher et al. 2013; Hwang and Frierson 2013). The forcing induced by the altered solar flux is time varying due to the seasonal and diurnal cycles of insolation. The annual mean of net top-of-atmosphere (TOA) radiative forcing integrated over the forcing domain is constrained to produce a total energy perturbation of approximately 0.8 PW, equivalent to 1.6 W m^{-2} in the global mean.

In a fully coupled system, the magnitude of the imposed forcing is difficult to estimate due to the

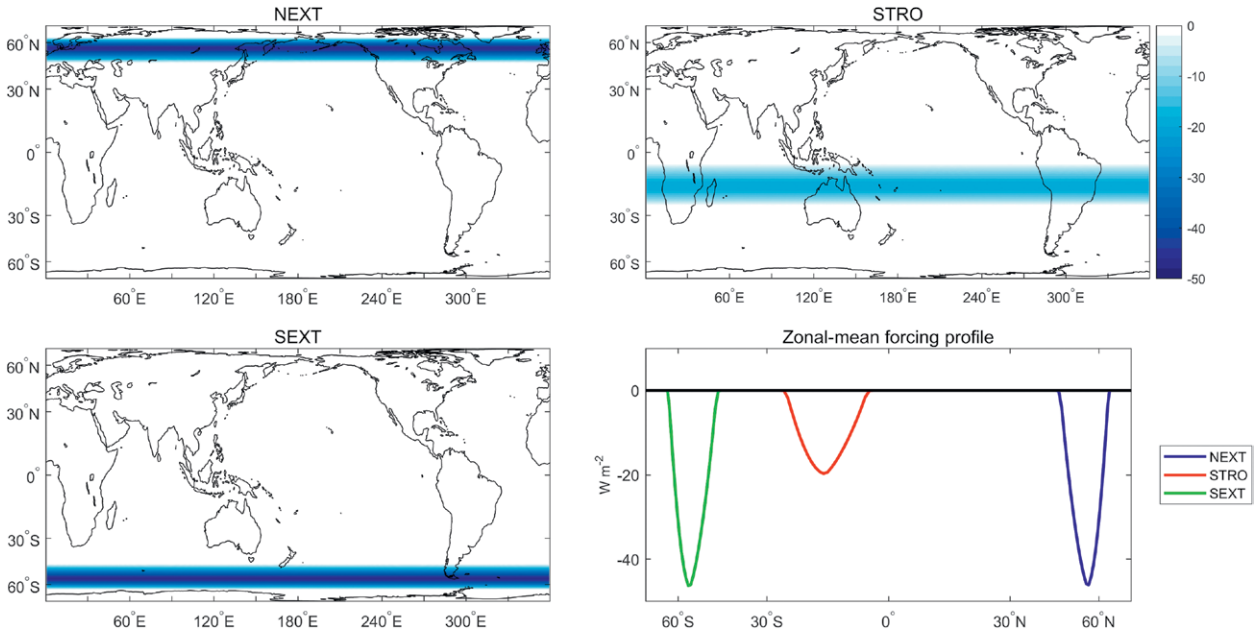

Fig. 1. The geographical distribution of solar flux perturbation.

slowly evolving SST and the associated feedbacks (Myhre et al. 2013). Furthermore, Forster et al. (2016) demonstrates that the effective radiative forcing diagnosed from fixed SST simulations is more accurate than that based on the regression method (Gregory et al. 2004). Therefore, we estimate the forcing magnitude based on model experiments with fixed SSTs using the GFDL Atmosphere Model, version 4 (AM4) (Zhao et al. 2018). AM4 integrated with the observed SST and sea ice concentration is perturbed by reducing solar flux as in one of the perturbation experiments. The difference of annual-mean TOA net shortwave radiation over the forcing domain between the control and perturbation experiments is set to be approximately 0.8 PW in GFDL AM4. Because of the intermodel differences in climatology of planetary albedo, the same perturbation in solar flux does not necessarily guarantee a forcing of same magnitude. Thus, we compute a weighting factor for each model experiment so as to adjust the prescribed solar flux perturbation multiplied by one minus the planetary albedo in CNTL of each model to 0.8 PW (Table ES1 in the online supplemental material: https://doi.org/10.1175/BAMS-D-18-0301.2). This weighting factor, which ranges between 0.80 and 1.13 depending on the forcing region and a model, is applied to any diagnostics in postprocessing prior to taking the multimodel mean. Keeping in mind that our original motivation is to address the double ITCZ bias in the mean state, we analyze the last 50-yr mean of 150-yr integrations of coupled model experiments because 1) the simulations reach a new quasi-equilibrium state after ~40 years based on the global imbalance of TOA radiation as well as net surface fluxes (Fig. ES1) and 2) 50 years is a long enough period to remove any signatures of decadal variability. Although the deep ocean would be far from reaching an equilibrium (Fig. ES2), we note that it is not critical for our purpose.

Additional tier 2 experiments are under development by a subset of models to further 1) examine sensitivity to the type of forcing (surface vs TOA), 2) enable direct comparison between fully coupled and slab ocean simulations, 3) examine linearity to forcing magnitude, 4) examine the asymmetric response to cooling and heating cases, and 5) separate rapid adjustments from feedback responses via fixed SST/sea ice experiments. These additional experiments will help to elaborate upon and evaluate the robustness of our findings. Any modeling groups interested in participating in either tier 1 or 2 are welcome to contact the corresponding author.

Given the focus of ETIN-MIP on energy budgets, the diagnostics required to compute meridional eddy heat and momentum fluxes for atmosphere and ocean are requested (see Table ES2 for descriptions). For ocean meridional mass and heat transport diagnostics, all parameterized components and meridional diffusion need to be provided. The variables in Table ES2 need to be calculated at every time step before performing any time averages. We request to output those variables at model levels (before interpolating to standard pressure levels) to better close the budget.

Table 1. Description of the nine ETIN-MIP models. The analysis of UCLA–MIT GCM is based on the average of last 20 years of 60-yr integrations. The analysis of NorESM1-HAPPI for NEXT is based on the average of last 30 years of 100-yr integration. The relatively insensitive climate response to time (Fig. ES1) justifies the inclusion of those simulation results in our analysis.

Model	Atmosphere resolution	Ocean resolution	Key reference	Note
Max Planck Institute Earth System Model (MPI-ESM1.2-LR)	T63 (1.875° × 1.875°), 47 levels	MPIOM1.6.3 (1.5°), 40 levels	Mauritsen et al. (2019); Müller et al. (2018)	
Hadley Centre Global Environment Model, version 2, Earth System (HadGEM2-ES)	1.875° × 1.25°, 38 levels	1° reducing to 1/3° at equator, 40 levels	Martin et al. (2011); Collins et al. (2011)	
Norwegian Earth System Model, version 1 (NorESM1-HAPPI)	0.94° × 1.25°, 26 levels	~1° and a displaced pole grid	Mitchell et al. (2017)	NEXT run for only 100 years
IPSL CM5A2	96 × 95 points, 39 levels	2° reducing to 1/2° at equator, 31 levels	Dufresne et al. (2013)	
GFDL AM4-FLOR	1° × 1°, 32 levels	1° × 1°, 50 levels	Xiang et al. (2018)	
GFDL CM2.1	2.5° × 2°, 24 levels	1° reducing to 1/3° at equator, 50 levels	Delworth et al. (2006)	
Community Earth System Model (CESM 1.2.2)	1.9° × 2.5°, 30 levels	1° (lon) and 0.6° reducing to 0.3° at equator (lat), 60 levels	Hurrell et al. (2013)	
Model for Interdisciplinary Research on Climate (MIROC5.2)	T85, 40 levels	1° × 1°, 63 levels	Watanabe et al. (2014)	STRO not available
UCLA–MIT GCM	2.5° × 2°, 29 levels	1° × 0.3° for 10°S–10°N 1° ×1° poleward 22°S/N, 46 levels	Cazes-Boezio et al. (2008)	Run for only 60 years

ETIN-MIP model output is provided in the standardized format taken from a subset of the CMIP5 output protocol. The time mean over the last 50 years of a subset of output can be obtained online (https://zenodo.org/record/3362615#.XU6585MzbOQ). A complete set of output, which is provided as 1) decadal means of each month for the entire simulation period, and 2) monthly means for the first and last 20 years of the simulation period, will be made available to the research community upon request to the corresponding author. Nine models participating in ETIN-MIP and their descriptions are in Table 1.

TOA ENERGY PERTURBATION AND CLIMATE RESPONSE. An initial finding from ETIN-MIP is that among the three forcing domains, the southern tropics is most efficient at driving a meridional shift and manipulating the equatorial peak of tropical precipitation (Fig. 2, left). The two extratropical forcing cases exhibit a clear meridional shift of tropical precipitation in the Atlantic and Indian Ocean, while a common equatorially concentrated drying response appears in the Pacific. The off-equatorial response in the Pacific features a meridional shift in NEXT while it is nearly symmetric in SEXT. To quantify these effects, we use the tropical precipitation asymmetry index (P_{ASY}), introduced by Hwang and Frierson (2013), and the equatorially symmetric precipitation index (P_{SYM}), introduced by Adam et al. (2016): P_{ASY}, the difference in the precipitation averaged between 0° and 20°N and that between 0° and 20°S normalized by the mean precipitation between 20°S and 20°N, measures the meridional shift; while P_{SYM}, the average precipitation over 2°S–2°N divided by that over 20°S–20°N minus 1 measures the relative magnitude of the equatorial peak. Changes in P_{ASY} and P_{SYM} as well as changes in total precipitation between 20°S and 20°N are shown in Fig. 3. For reference, overlaid with CNTL as a gray star symbol is the observed value based on Global Precipitation Climatology Project (GPCP) data averaged between 1980 and 1999. The results clearly show that the imprint of TOA energy biases on tropical precipitation differs depending on the geographic location of the bias.

Figure 4 shows the global surface temperature response to the prescribed TOA cooling in the three perturbation experiments. The local cooling response over the forcing domain is most pronounced in NEXT (−4.00 K) while the forcing domains are cooled

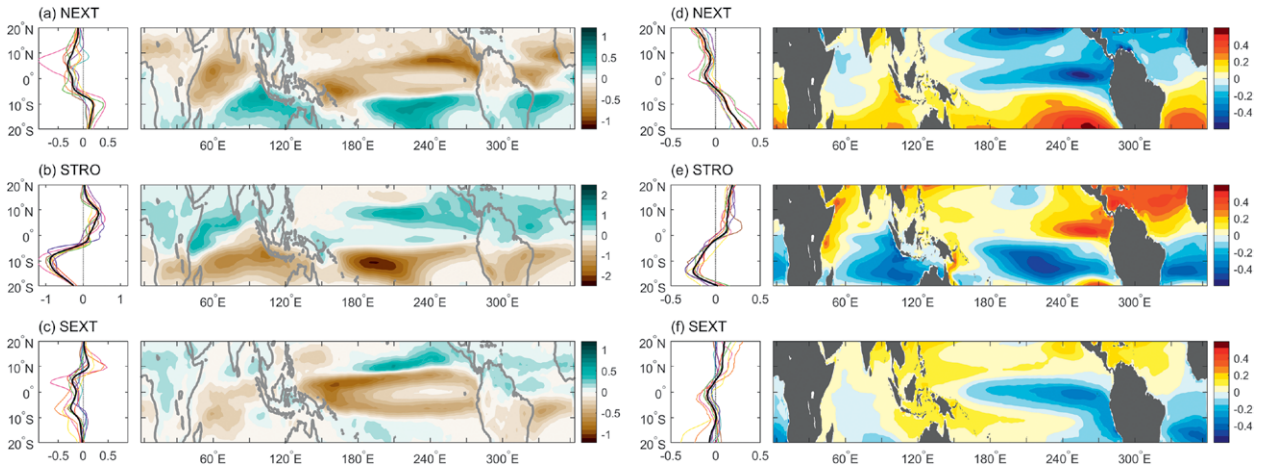

Fig. 2. Geographical distributions of the multimodel and annual mean changes in (a)–(c) precipitation (mm day^{-1}) and (d)–(f) relative SST (defined as the SST subtracted from the tropical mean SST between 20°S and 20°N, in K), and their zonal-mean profiles over 20°S and 20°N. In the zonal-mean plots, the individual models are color coded as in Fig. 3 and the multimodel mean is shown in black. Note the differing scale in the zonal-mean precipitation response.

significantly less in the other two experiments with −1.92 in SEXT and −0.89 in STRO. Although STRO exhibits only a weak interhemispheric contrast in the surface temperature response (Fig. 4, left), it exhibits the largest meridional gradient of SST anomalies within 20°S and 20°N (Fig. 2, right). Consequently, STRO induces the strongest cross-equatorial Hadley circulation anomalies (Fig. 4, right) and the largest meridional shift of tropical precipitation (Fig. 2, left). Figure 5a shows that the interhemispheric difference of tropical SST response is positively correlated with P_{ASY} response. When all model experiments are considered, 85% of the intermodel variance of P_{ASY} response is explained by variations in the meridional gradient of tropical SST anomalies. The variance of P_{ASY} response is nearly as well correlated with the cross-equatorial atmospheric energy transport anomalies (F_{ATM0}), even within each experiment (Fig. 5b). This suggests that the ITCZ shift, atmospheric energy transport and tropical SST changes are strongly coupled with each other. Given this, we proceed to explain the intermodel spread of P_{ASY} response by investigating the cause of the intermodel spread of F_{ATM0} through examining the atmospheric energy budget.

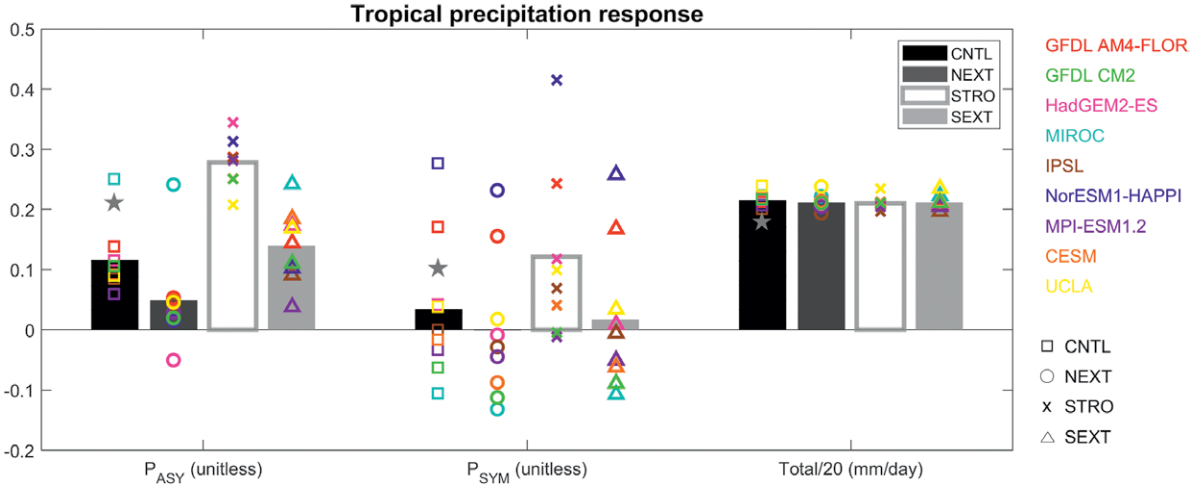

Fig. 3. The tropical precipitation asymmetry index P_{ASY} (the difference in the precipitation averaged between 0° and 20°N and that between 0° and 20°S normalized by the mean precipitation between 20°S and 20°N), the equatorial precipitation index P_{SYM} (the average precipitation over 2°S–2°N divided by that over 20°S–20°N minus 1), and the area-averaged precipitation between 20°S and 20°N divided by a factor of 20 (in mm day^{-1}). The gray star symbol overlaid with CNTL is the observed value based on Global Precipitation Climatology Project (GPCP) data averaged between 1980 and 1999.

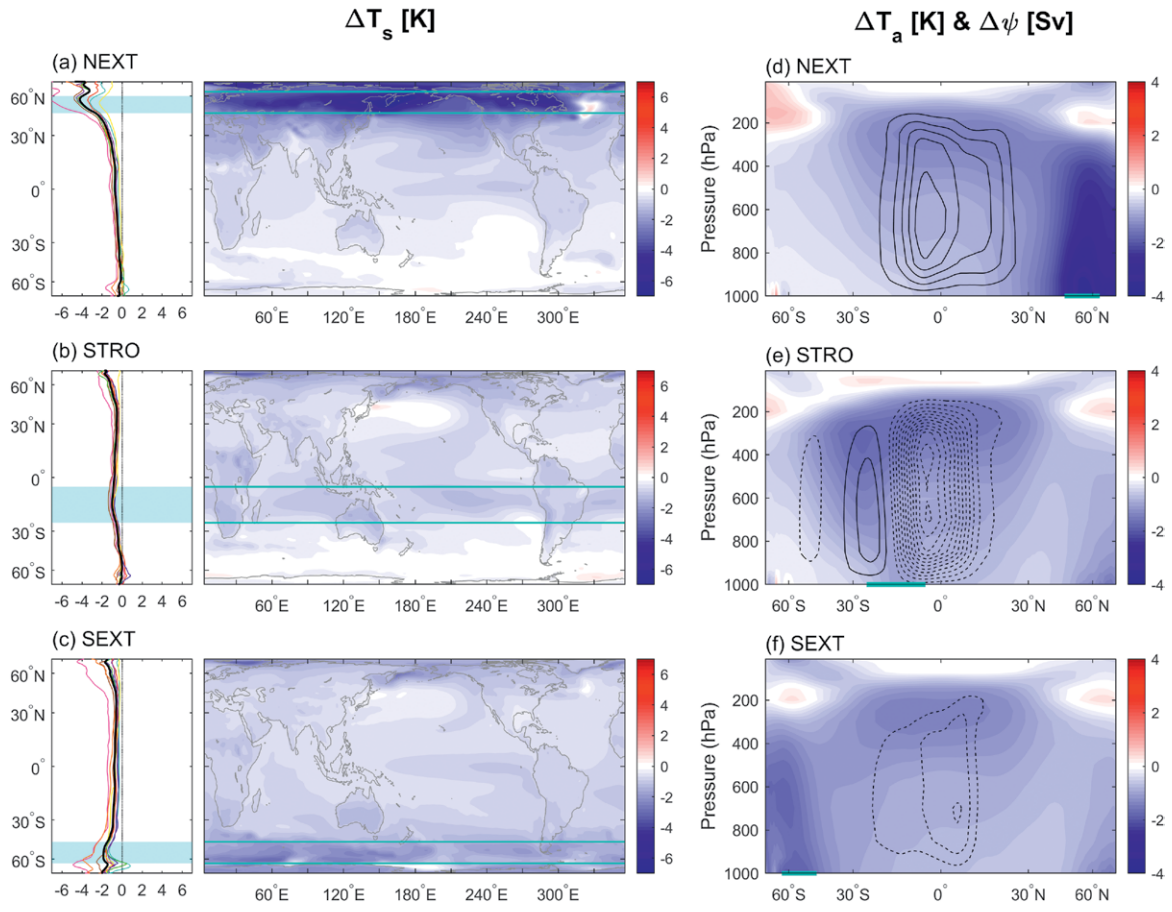

FIG. 4. Geographical distributions of (a)–(c) the multimodel and annual mean changes in global surface temperature (in K) and its zonal-mean profile, and (d)–(f) the multimodel, zonal and annual mean temperature changes (shading; in K) and anomalous meridional streamfunction (contours interval = 3 × 10^9 kg s^{-1}). Solid (dashed) contour indicates a clockwise (counterclockwise) circulation. In the zonal-mean plots, the individual models are color coded as in Fig. 3 and the multimodel mean is shown in black.

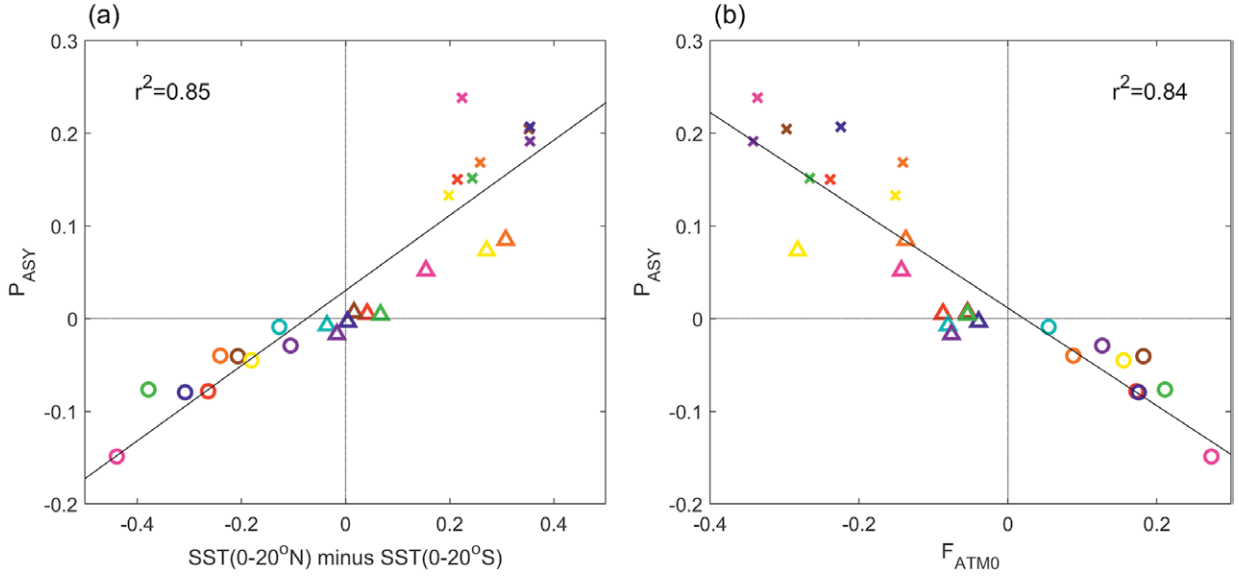

FIG. 5. Scatterplot of the precipitation asymmetry index (P_{ASY}) response (unitless) vs (a) the interhemispheric difference of sea surface temperature response over 20°S–20°N (in K) and (b) the anomalous cross-equatorial atmospheric energy transport F_{ATM0} (in PW). The individual models are color coded as in Fig. 3.

TROPICAL PRECIPITATION RESPONSE AND ATMOSPHERIC ENERGY BUDGET. The extent to which the TOA energy perturbations induce a meridional shift of tropical precipitation is controlled by processes that determine the atmospheric energy budget in an equilibrium state:

$$E_{\mathrm{TOA}} - E_{\mathrm{OCN}} = \nabla \cdot F_{\mathrm{ATM}}, \qquad (1)$$

where all quantities indicate the climatological difference between the perturbed and CNTL experiments. Note that the atmospheric energy storage can be neglected when diagnosing the quasi-equilibrated annual-mean response. Here, E_{TOA} is the anomalous net downward radiation at TOA, E_{OCN} is the anomalous net downward surface energy flux, and F_{ATM} is the anomalous northward atmospheric energy transport. Equation (1) states that net atmospheric column energy input through the TOA and ocean surface is balanced by a divergence of atmospheric energy transport.

The anomalous net downward radiation at TOA, E_{TOA} includes the prescribed forcing, which is the fraction of solar flux perturbation ΔS felt by the system, $E_S \equiv (1 - \alpha)\Delta S$, where α is the climatological mean planetary albedo in CNTL. As mentioned earlier, the magnitude of prescribed forcing across models may differ due to model differences in α; thus, the weighting factor in Table ES1 is accounted for to adjust the forcing magnitude to 0.8 PW in all models. The difference between E_{TOA} and the prescribed forcing is referred to as the TOA response (denoted as $E_{\mathrm{TOA-}S}$), taking into account both rapid adjustments, which modify the radiative budget indirectly through fast atmospheric and surface changes, and feedbacks, which operate through changes in climate variables that are mediated by surface temperature changes (Sherwood et al. 2015). The anomalous net surface energy flux E_{OCN} represents heat uptake by the ocean, which involves both ocean heat storage and ocean heat transport divergence (W. Liu et al. 2018). In a slab ocean setting where SSTs are computed based on the local surface energy budget while neglecting ocean dynamics, the net surface energy flux response E_{OCN} is zero by construction. In a fully coupled setting, the net surface energy flux response E_{OCN} can be shaped by distinct oceanic processes that take place on different time scales. Within the first decade, Ekman transport arising from the coupling between the Hadley circulation and the oceanic subtropical cells as well as gyre circulations formed by the surface wind patterns are primarily responsible for ocean heat uptake changes E_{OCN} (Fig. ES3). Slow ocean processes associated with deep overturning circulation also play an important role in altering E_{OCN}, but the adjustment time scale varies considerably depending on the forcing region. For example, the Atlantic meridional overturning circulation (AMOC) strength adjusts after approximately 50 years in NEXT while it steadily increases for the entire simulation period of 150 years in SEXT (Fig. ES2). In addition to versions of oceanic circulations, the prescribed forcing may also influence the ocean heat uptake response E_{OCN} and the associated SST pattern via anomalous advection by the mean circulation, which is a process on decadal time scales (Li et al. 2013; Wang et al. 2018). That is, during the last 50-yr period that we analyze here, multiple ocean processes play a role in shaping E_{OCN}. Attribution of E_{OCN} to different oceanic processes is a challenging topic to be further explored.

To obtain an equation for the cross-equatorial atmospheric energy transport anomalies F_{ATM0}, which is shown to be strongly correlated with the ITCZ shift (Fig. 5b), we reformulate Eq. (1) to depict the hemispheric asymmetry by spatially integrating over the Southern Hemisphere with the global mean removed:

$$\langle E_S \rangle = -\langle E_{\mathrm{TOA-}S} \rangle + \langle E_{\mathrm{OCN}} \rangle + F_{\mathrm{ATM0}}, \qquad (2)$$

where brackets denote the spatial integral of the anomaly from the global mean over the Southern Hemisphere. All variables have the units in watts. Equation (2) indicates that the hemispheric asymmetry in prescribed forcing $\langle E_S \rangle$ is balanced by adjusting the hemispheric asymmetry in TOA radiation response $\langle E_{\mathrm{TOA-}S} \rangle$ and ocean heat uptake response $\langle E_{\mathrm{OCN}} \rangle$, and the cross-equatorial atmospheric energy transport response F_{ATM0} (Fig. 6a). We define the fraction of prescribed forcing balanced by each component as the TOA compensation, oceanic compensation, and atmospheric compensation:

$$C_{\mathrm{TOA}} \equiv \frac{\langle -E_{\mathrm{TOA-}S} \rangle}{\langle E_S \rangle}, \quad C_{\mathrm{OCN}} \equiv \frac{\langle E_{\mathrm{OCN}} \rangle}{\langle E_S \rangle},$$
$$\text{and} \quad C_{\mathrm{ATM}} \equiv \frac{F_{\mathrm{ATM0}}}{\langle E_S \rangle},$$

such that $C_{\mathrm{TOA}} + C_{\mathrm{OCN}} + C_{\mathrm{ATM}} = 1$.

Figure 7 compares the fractional compensation by each component in all model experiments. Consistent with the sensitivity of P_{ASY} response to the location of forcing domains, all models exhibit the largest C_{ATM} in STRO associated with the smallest C_{OCN}. This implies that radiation biases over the tropics are more effective in driving the spurious double ITCZ problem in current climate models than extratropical radiation biases (Hawcroft et al. 2018; Xiang

et al. 2017, 2018; Green et al. 2019). A relatively smaller C_{ATM} for the extratropical experiments is associated with a larger C_{OCN} while the contribution from radiative adjustment (C_{TOA}) is small and highly uncertain in terms of sign. Comparing the two extratropical experiments, NEXT induces a slightly larger C_{ATM} than SEXT in the multimodel mean, consistent with a stronger cross-equatorial Hadley circulation in NEXT (Fig. 4, right). However, this sensitivity to the forced hemisphere is model dependent, with three out of nine models exhibiting the opposite sensitivity with a larger C_{ATM} in SEXT. The causes of these differences are a topic of planned future research within ETIN-MIP.

Recent studies attribute the muted tropical precipitation responses to extratropical energy perturbations in fully coupled models to oceanic processes (Deser et al. 2015; Kay et al. 2016; Green and Marshall 2017). The oceanic compensation C_{OCN} is zero in a slab ocean setting by construction; hence, a larger fraction of energy perturbations must be balanced by the atmospheric energy transport compared to the case when coupled to a full ocean model. Some studies point to the coupling between the Hadley circulation and the oceanic subtropical cells for the reduced tropical precipitation responses (Green and Marshall 2017; Schneider 2017; Kang et al. 2018a; Green et al. 2019). Ekman coupling ensures that the Hadley circulation and the oceanic subtropical cells transport the anomalous energy in the same direction, thereby damping the ITCZ response. If Ekman coupling is the primary factor in the oceanic damping effect, STRO is expected to exhibit the largest oceanic compensation C_{OCN} considering that the anomalous Hadley cell strength is by far strongest (Fig. 4, right), yet

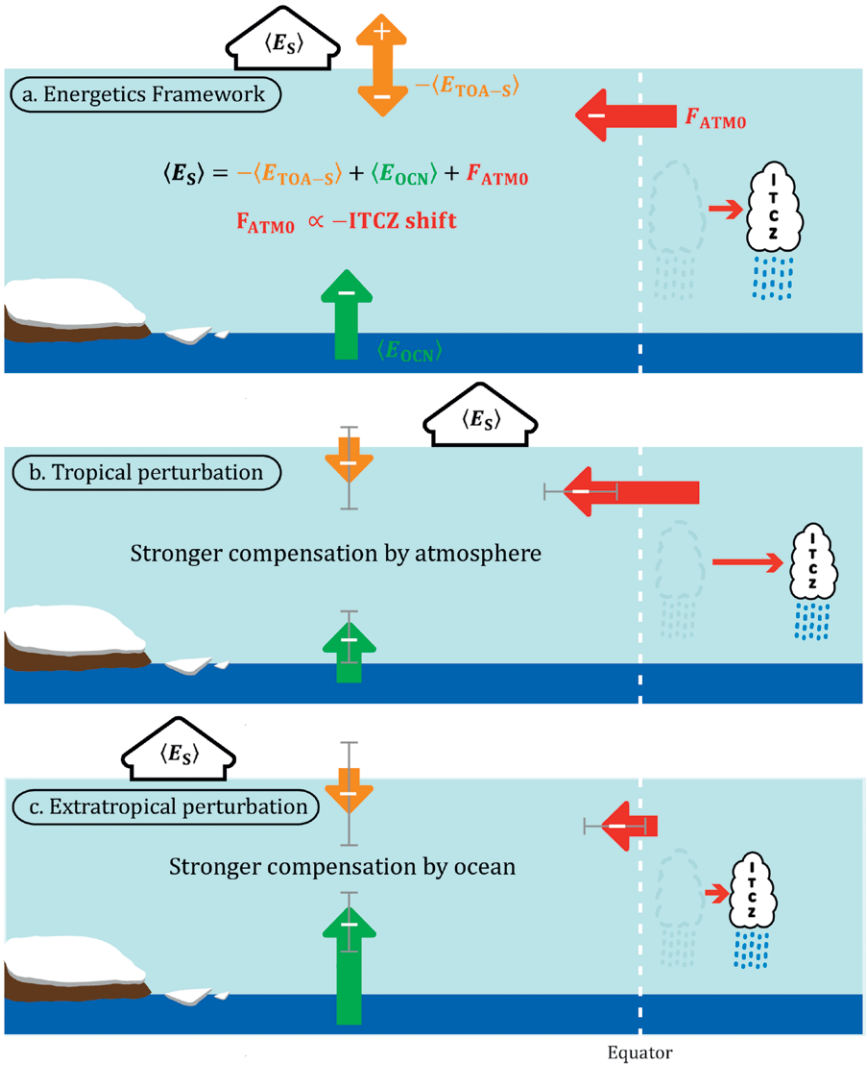

Fig. 6. Schematic diagram of the energy fluxes and ITCZ shift. Minus sign in the colored arrows indicates that the given process compensates the prescribed forcing (acting as a negative feedback) while plus sign indicates that the given process amplifies the prescribed forcing (acting as a positive feedback). Gray bars in the colored arrows in (b) and (c) denote the model spread from ETIN-MIP. (a) A solar flux reduction in the Southern Hemisphere (black open arrow) is balanced by the upward ocean heat uptake response E_{OCN} (green arrow) and a southward cross-equatorial atmospheric energy transport response F_{ATM0} (red arrow) while the TOA radiation response E_{TOA} may act as either dampener or amplifier of forcing (orange arrow). A southward F_{ATM0} is associated with a northward ITCZ shift. (b) Energy flux and ITCZ response to a solar flux reduction in the southern tropics. The forcing is balanced more by F_{ATM0}, leading to a large ITCZ shift. (c) Energy flux and ITCZ response to a solar flux reduction in the southern extratropics. The forcing is damped effectively by ocean heat uptake response over the Southern Ocean, accompanying a small F_{ATM0} and a muted ITCZ shift.

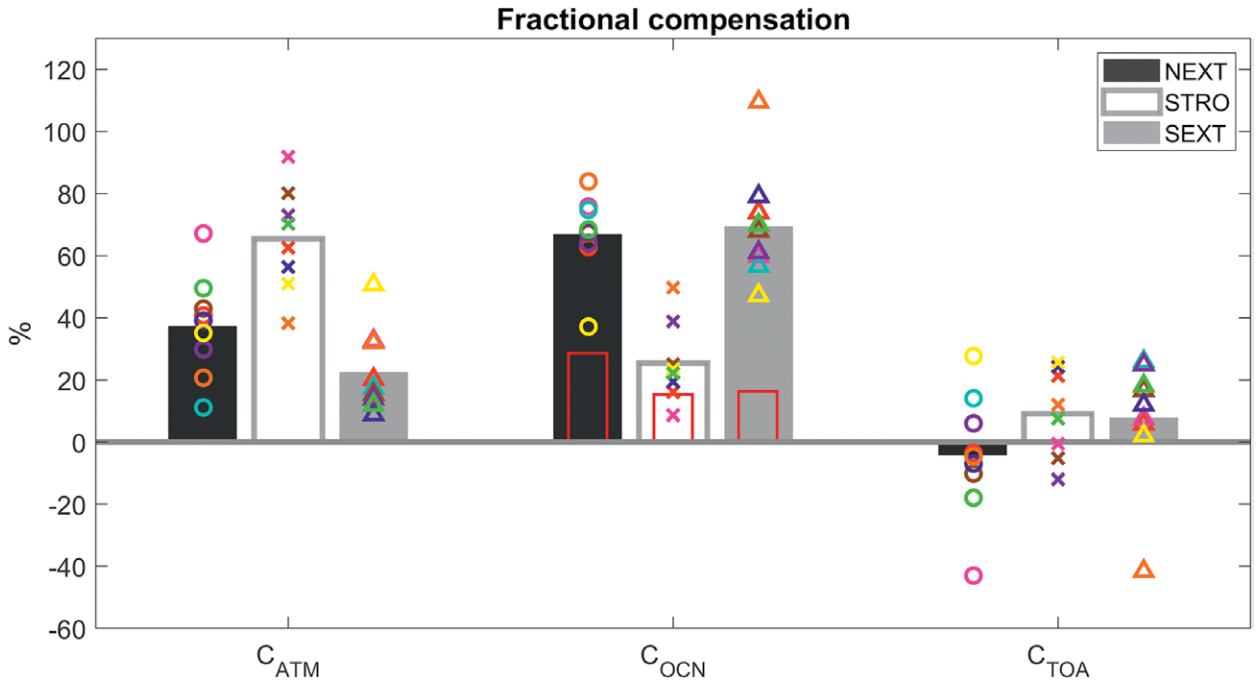

FIG. 7. The fractional compensation (in %) by the atmospheric energy transport (C_{ATM}), the ocean heat uptake (C_{OCN}), and the TOA radiation (C_{TOA}) at the equator. The oceanic compensation accomplished within 30°S–30°N is displayed in red bars. The individual models are color coded as in Fig. 3.

STRO exhibits the smallest C_{OCN} (Fig. 7). The Ekman damping effect by the oceanic subtropical cells should be included in the fraction of C_{OCN} resulting from the ocean heat uptake response within the tropics. Red bars in Fig. 7 display the tropical component of C_{OCN}, computed by taking into account E_{OCN} between 30°S and 30°N in isolation. The tropical C_{OCN} in STRO is smaller than that in NEXT by 48% despite a significantly stronger anomalous Hadley circulation in STRO (Fig. 4, right). In addition, STRO and SEXT exhibit a comparable tropical C_{OCN} despite a stark contrast in the anomalous Hadley cell strength. The result not only implicates other potentially important oceanic damping pathways than the Ekman transport but also suggests a limited ability of the ocean's Ekman transport to compensate the energy perturbations, potentially due to small gross stability in the shallow ocean mixed layer (Kang et al. 2018b).

A question then arises as to which oceanic processes are responsible for modulating the oceanic compensation. Figure 8 shows that E_{OCN} in NEXT primarily occurs in the subpolar North Atlantic and along the western boundary currents while that in SEXT primarily occurs in the Southern Ocean. Indeed, the full C_{OCN} in the extratropical experiments is dominated by the extratropical component (Fig. 7). In other words, it is the extratropical oceanic processes that boost the oceanic compensation in the extratropical experiments, thereby shaping the overall sensitivity of C_{OCN} to forcing region (Yu and Pritchard 2019). To examine the origin of E_{OCN}, Fig. 9 compares the anomalous ocean meridional overturning circulation (MOC) streamfunction and the mean ocean temperature in CNTL on the left column with the anomalous ocean temperature and the mean ocean MOC streamfunction in CNTL on the right column. The left column allows an estimation of the ocean heat transport change resulting from ocean circulation changes (i.e., the dynamic term) while the right column allows an estimation of that resulting from ocean temperature changes (i.e., the thermodynamic term). In NEXT, the subpolar North Atlantic E_{OCN} results from the dynamic term associated with a strengthened AMOC (Fig. 9a) while the Southern Ocean E_{OCN} in SEXT results from the thermodynamic term associated with the mean upward motion at 50°–60°S (Fig. 9f) (Bryan et al. 1988; Armour et al. 2016; Frey et al. 2017; Xiang et al. 2018). This local ocean heat uptake response E_{OCN} over the forced latitude band is larger in SEXT than in NEXT for all models, by a factor of 1.64 in the multimodel mean (Fig. 8, left). However, remote oceanic processes outside of the forcing region as well as its interaction with radiative feedbacks add uncertainty to the sensitivity of C_{OCN}, with it being larger in SEXT for only two thirds of the models and

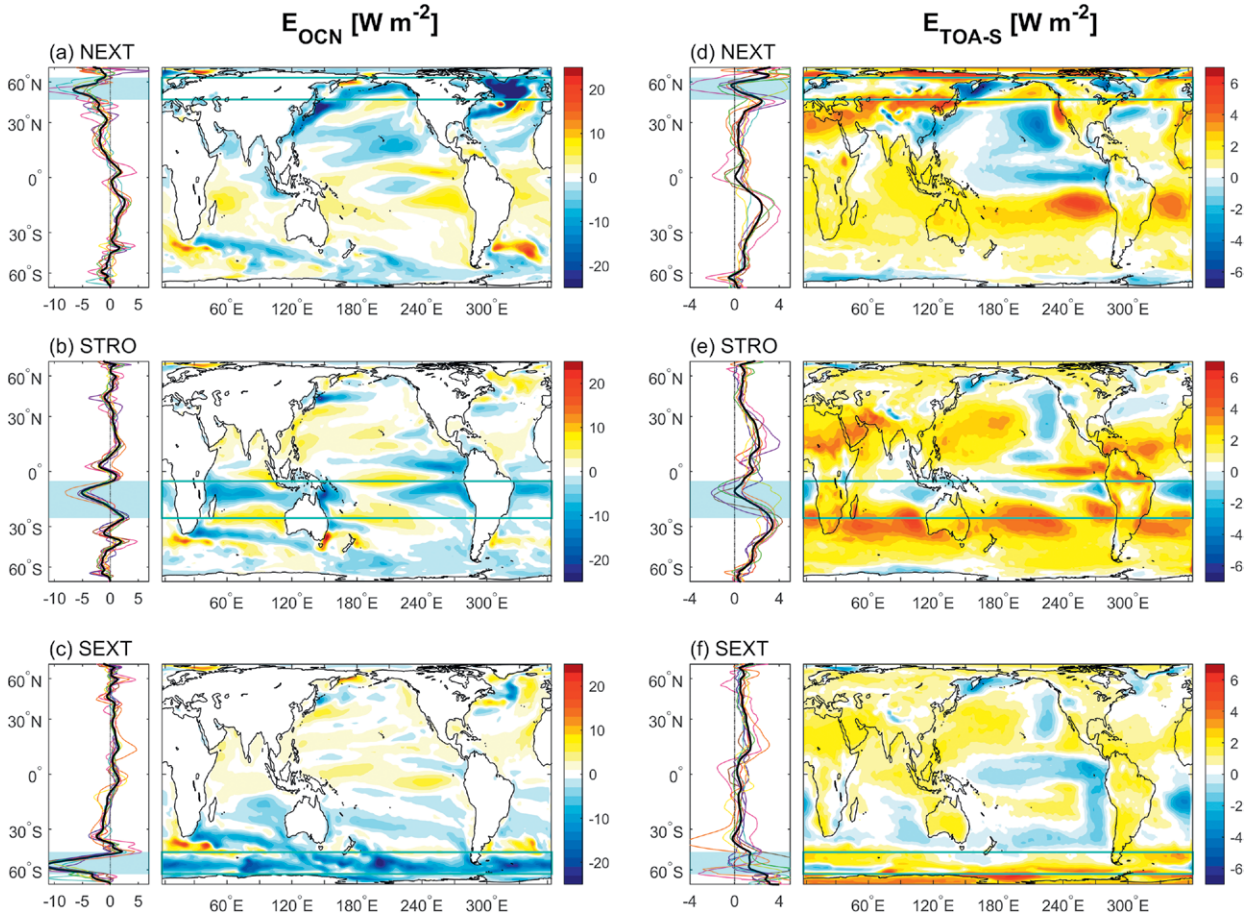

FIG. 8. Geographical distribution of the multimodel and annual mean changes in (a)–(c) net downward surface heat flux E_{OCN} and (d)–(f) effective net TOA radiation E_{TOA-S} and their zonal-mean profiles. Both E_{OCN} and E_{TOA-S} are defined positive downward. In the zonal-mean plots, the individual models are color coded as in Fig. 3 and the multimodel mean is shown in black.

a third exhibiting the opposite sensitivity (Fig. 7). In STRO, an anomalously anticlockwise circulation in the southern tropical upper ocean (Fig. 9b) gives rise to a southward ocean heat transport, which is largely cancelled by the thermodynamic term associated with the subsurface warming driven by the anomalous downwelling (Fig. 9e). As a result, the equatorial C_{OCN} in STRO is small relative to the extratropical cases (Fig. 7) (Xiang et al. 2018; Hawcroft et al. 2018). The ETIN-MIP output will allow a rigorous decomposition of the anomalous ocean heat transport into the thermodynamic and dynamic terms.

The TOA compensation C_{TOA} is highly uncertain for all experiments, resulting in a near-zero C_{TOA} in the multimodel mean with a large intermodel spread (Fig. 7). A large diversity in C_{TOA} originates from multiple factors such as rapid adjustment and climate feedbacks associated with clouds, water vapor, surface albedo, and Planck response. For the purpose of separating the contribution of rapid adjustment to the diversity of C_{TOA} from contribution of climate feedbacks, we plan to perform fixed SST/sea ice experiments for tier 2. Potential factors responsible for the large intermodel spread of C_{TOA} is the uncertainty in sea ice and cloud responses. Since the ice-albedo feedback and shortwave low-cloud feedback become weak during the winter months, we weight the monthly changes in sea ice and low cloud cover by monthly insolation before taking the annual mean in Fig. 10. In NEXT, HadGEM2-ES exhibits the largest increase in sea ice cover over the northern high latitudes (Fig. 10a), which greatly amplifies the forcing effect, so that the radiative adjustment acts as a positive feedback rather than a compensating effect (i.e., $C_{TOA} < 0$) (Fig. 7). In the extratropical cases, the low cloud cover tends to increase within and equatorward of the forced latitude band (Figs. 10d,f), due to an increase in lower-tropospheric stability associated with a cooler boundary layer (Wood and Bretherton 2006). In

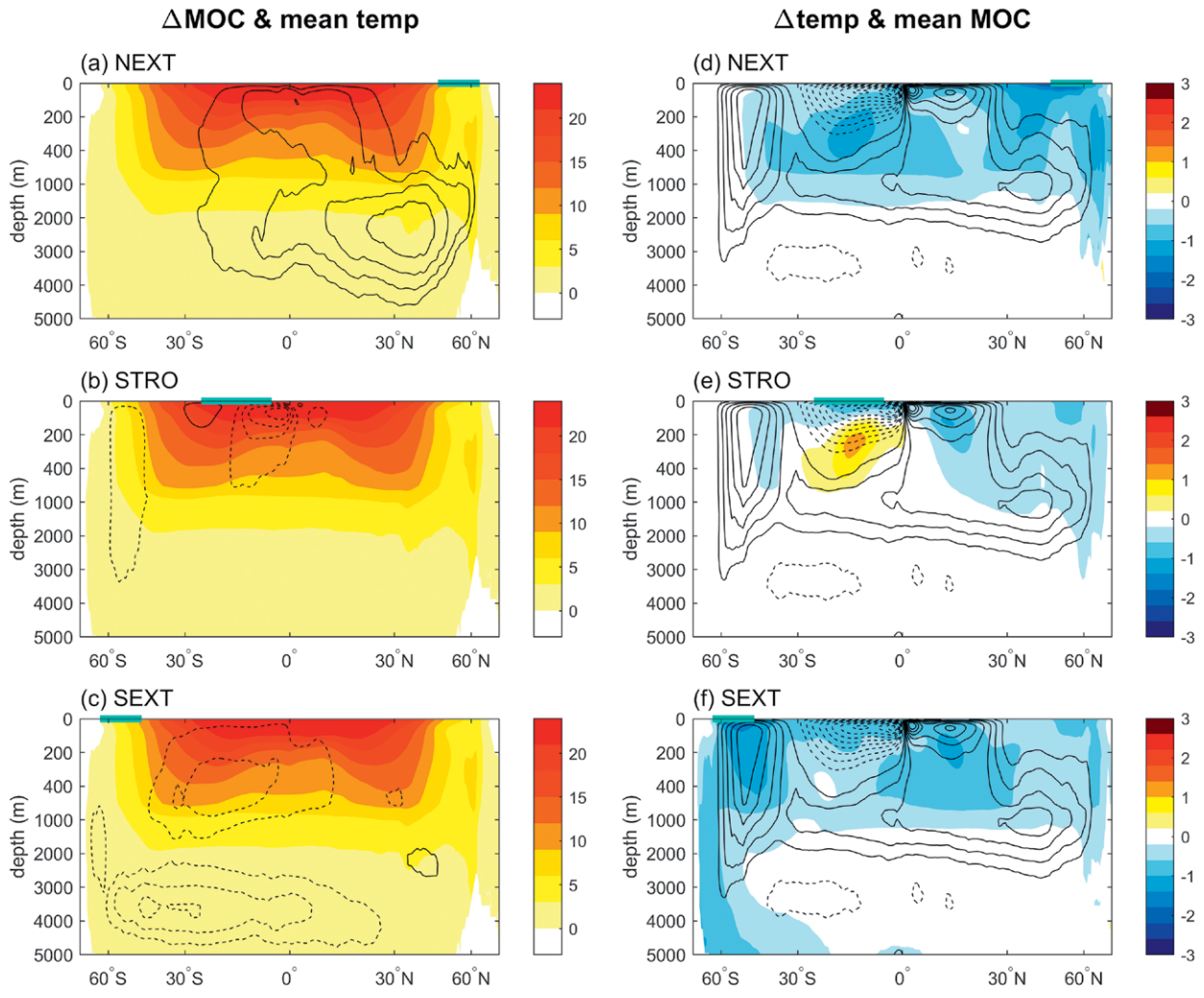

Fig. 9. (a)–(c) The multimodel and annual mean ocean temperature in CNTL (shading; in K) and ocean MOC streamfunction changes (contour interval = 2 Sv) (1 Sv ≡ 10^6 m^3 s^{-1}). Solid (dashed) contour indicates a clockwise (counterclockwise) circulation. (d)–(f) The multimodel and annual mean ocean temperature changes (shading; in K) and the ocean MOC streamfunction in CNTL (contour interval = 5 Sv).

SEXT, NCAR CESM exhibits the largest low cloud cover increase in the southern subtropics to midlatitudes, which enhances the reflected shortwave radiation thereby amplifying the forcing effect, while MPI-ESM1.2 exhibits the smallest changes in low cloud cover. This is consistent with negative C_{TOA} in NCAR CESM and positive in MPI-ESM1.2 (Fig. 7). HadGEM2-ES in SEXT exhibits a hemispherically symmetric response in both sea ice and low cloud cover relative to other models (Figs. 10c,f), so that the radiative compensation C_{TOA} is nearly zero (Fig. 7). An ETIN-MIP study under development will apply the approximate partial radiative perturbation method (Taylor et al. 2007) and kernel method (Pendergrass et al. 2018) to investigate the cause of intermodel diversity of TOA compensation and its dependence on forcing location.

BROADER IMPLICATIONS. A primary motivation for ETIN-MIP is to identify the remote energy biases that are potentially important for causing the double ITCZ bias. Understanding how regional energy perturbations affect the tropical precipitation pattern is of fundamental importance for improving not only the present-day double ITCZ bias in many current climate models but also the accuracy of projections of future changes in tropical precipitation due to the uneven regional distribution of warming (e.g., Arctic amplification; Serreze and Barry 2011; Screen et al. 2018).

Applying a forcing over finite latitudinal bands in a coupled model framework, similar to the ETIN-MIP experiment configuration, has proven to be useful for determining the causes of climate change patterns (Stuecker et al. 2018). We envision ETIN-MIP can

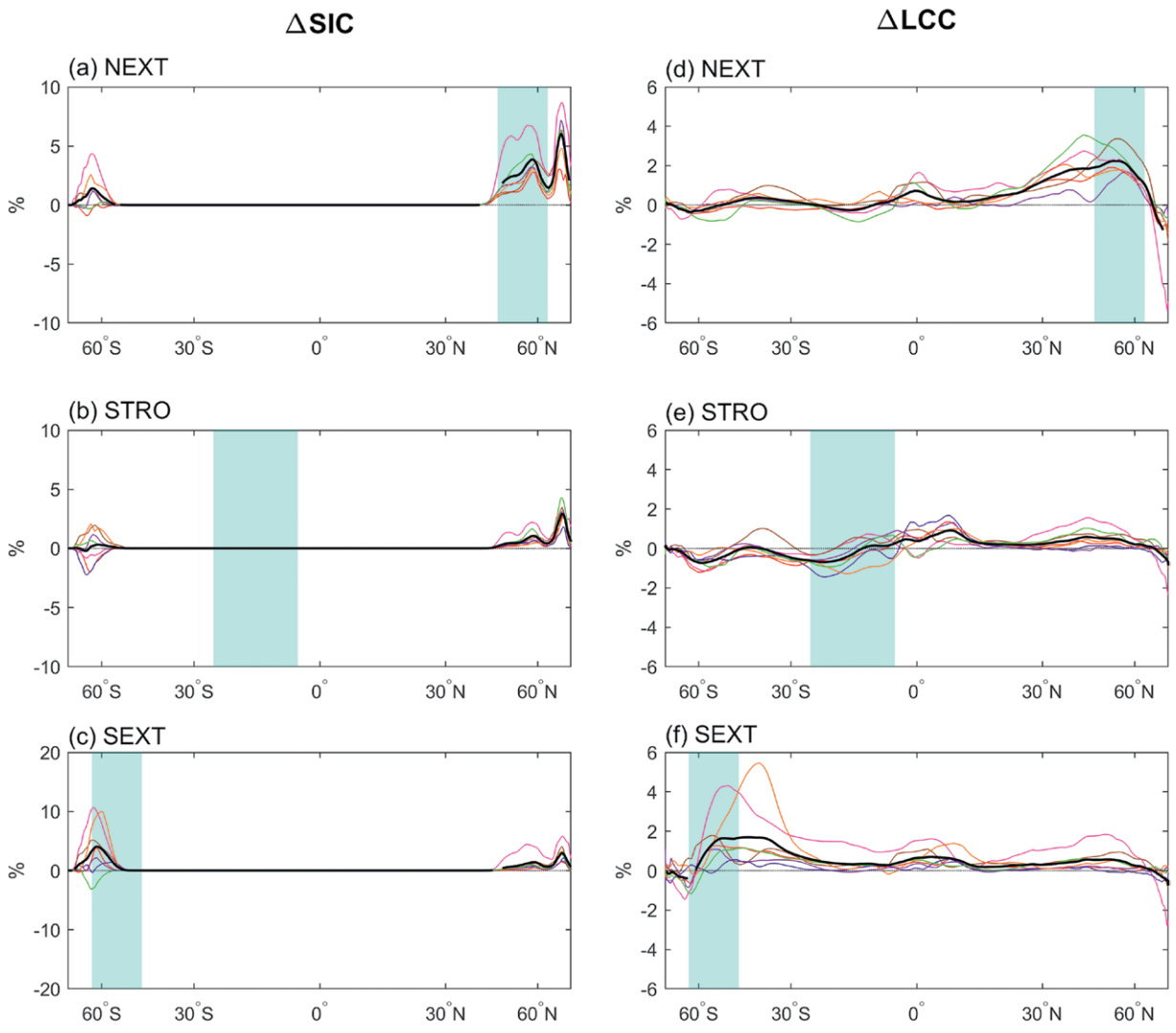

Fig. 10. Zonal and annual mean changes in (a)–(c) sea ice fraction (in %) and (d)–(f) low cloud cover (in %), for the selected models where the variables were made available. For both variables, the monthly changes are weighted by the monthly insolation before taking the annual mean. The individual models are color coded as in Fig. 3 and the multimodel mean is shown in black

be generalized to study other aspects of the climate response beyond tropical precipitation. First, understanding how the spatial pattern of tropical Pacific SST evolves within ETIN-MIP will provide insights relevant for a current topic of controversy—whether the equatorial Pacific under global warming would warm more in the east than the west (i.e., El Niño–like) or the reverse (e.g., Kohyama et al. 2017). Second, we plan to investigate how regional energy perturbations/biases influence the major climate modes such as El Niño–Southern Oscillation (e.g., Timmermann et al. 2007), which will help understand their future projections under radiative forcing with complex spatial patterns. Third, ETIN-MIP data are suitable for exploring one of the intriguing unanswered questions about Earth's albedo: the hemispheric symmetry in planetary albedo despite a substantial hemispheric asymmetry in clear-sky albedo (Voigt et al. 2013). Furthermore, ETIN-MIP experiments can be examined within the context of geoengineering where injecting stratospheric sulfate aerosols is proposed as a potential means of deliberately offsetting the global warming effect (Crutzen 2006; Jones et al. 2017). For example, ETIN-MIP results may highlight regions where geoengineering techniques may be applied for specific climate change mitigation effects to be maximized. Thus, the project encourages the wider research community to use the ETIN-MIP dataset for evaluating and understanding the global manifestation of regional energy perturbations, which can be viewed as energetics biases, anthropogenic forcings, or geoengineering applications.

SUMMARY. In ETIN-MIP, nine climate modeling groups have performed common numerical experiments aimed at enhancing our understanding of the mechanisms for two-way extratropics–tropics interactions. The link between the extratropics and tropics is of high societal concern given its role in controlling regional patterns of climate change. Improving our understanding of the mechanisms that enable these connections would significantly enhance our ability to predict and prepare for future changes in regional hydrology. The spirit of ETIN-MIP is strongly in line with one of the four questions of the World Climate Research Programme's Grand Challenge on Clouds, Circulation and Climate Sensitivity (Bony et al. 2015).

In keeping with the original motivation for ETIN-MIP, namely, to provide guidance on identifying the origin of the double ITCZ bias, we have presented initial results focused on tropical precipitation and energetics. The results have practical implications for GCM development strategy and suggest that fixing tropical biases would be a more viable option for alleviating hemispherically antisymmetric components of tropical precipitation biases while fixing extratropical biases is more desirable for improving the hemispherically symmetric component of tropical precipitation biases. It also implies that the ability of extratropical biases to manifest the hemispherically antisymmetric component of the double ITCZ bias would depend on the strength of stratocumulus–SST feedback in the subtropics (Mechoso et al. 2016). For example, the effect of extratropical biases diminishes away from the source region, but the rate of damping would be weaker in models with a stronger coupling between the subtropical stratocumulus and SST that acts as a positive feedback; hence, extratropical biases are able to project onto the double ITCZ bias in some models. The limited ability of extratropical biases to meridionally displace the tropical precipitation compared to tropical biases is due to efficient heat uptake response by extratropical oceanic processes (Figs. 6 and 7). It suggests constraining tropical response to regional energy perturbations requires improved understanding of deep ocean circulation response. This project will enhance our understanding of the origin of longstanding double ITCZ bias, which is an essential first step in informing model developers. More generally, ETIN-MIP will advance our physical understanding of the atmospheric and oceanic circulation responses to regional energy perturbations in a fully coupled framework, and provides a resource for the climate dynamics community to understand the plausibility of different model responses to such regionally varying energy perturbations, including those expected from anthropogenic climate change.

ACKNOWLEDGEMENTS. SMK, HK, and JK were supported by National Research Foundation of Korea (2017K2A9A1A06056874). MH is currently supported by the Queensland Government and Meat and Livestock Australia Donor Co. (MDC) through the Northern Australia Climate Program (NACP). YTH was supported by Ministry of Science and Technology in Taiwan (108-2636-M-002-007 and 106-2923-M-002-007-MY2). ØH and GM are supported by the project HYPRE (243942) funded through the Research Council of Norway, and NorESM1-HAPPI supercomputing resources have been provided by NOTUR (nn9188k). TL was supported by the Spanish Project CGL2017-86415-R. ØS was supported by the Norwegian Research Council, Project 261821 (HappiEVA). SY was supported by research grants from the NSF (AGS-1419518) and NASA (NNX17AH21G). CESM1.2 model simulations were performed on Cheyenne (ark:/85065/d7wd3xhc) provided by the NCAR's CISL, sponsored by the NSF.

REFERENCES

Adam, O., T. Schneider, F. Brient, and T. Bischoff, 2016: Relation of the double-ITCZ bias to the atmospheric energy budget in climate models: Double-ITCZ bias and atmospheric energy budget. *Geophys. Res. Lett.*, **43**, 7670–7677, https://doi.org/10.1002/2016GL069465.

Armour, K. C., J. Marshall, J. R. Scott, A. Donohoe, and E. R. Newsom, 2016: Southern Ocean warming delayed by circumpolar upwelling and equatorward transport. *Nat. Geosci.*, **9**, 549–554, https://doi.org/10.1038/ngeo2731.

Bellucci, A., S. Gualdi, and A. Navarra, 2010: The double-ITCZ syndrome in coupled general circulation models: The role of large-scale vertical circulation regimes. *J. Climate*, **23**, 1127–1145, https://doi.org/10.1175/2009JCLI3002.1.

Bony, S., and Coauthors, 2015: Clouds, circulation and climate sensitivity. *Nat. Geosci.*, **8**, 261–268, https://doi.org/10.1038/ngeo2398.

Boucher, O., and Coauthors, 2013: Clouds and aerosols. *Climate Change 2013: The Physical Science Basis*, T. F. Stocker et al., Eds., Cambridge University Press, 571–657.

Broccoli, A. J., K. A. Dahl, and R. J. Stouffer, 2006: Response of the ITCZ to Northern Hemisphere cooling. *Geophys. Res. Lett.*, **33**, L01702, https://doi.org/10.1029/2005GL024546.

Bryan, K., S. Manabe, and J. Spelman, 1988: Interhemispheric asymmetry in the transient response of a coupled ocean–atmosphere model to a CO_2 forcing. *J. Phys. Oceanogr.*, **18**, 851–867, https://doi.org/10.1175/1520-0485(1988)018<0851:IAITTR>2.0.CO;2.

Cazes-Boezio, G., D. Menemenlis, and C. R. Mechoso, 2008: Impact of ECCO ocean-state estimates on the initialization of seasonal climate forecasts. *J. Climate*, **21**, 1929–1947, https://doi.org/10.1175/2007JCLI1574.1.

Ceppi, P., Y.-T. Hwang, X. Liu, D. M. W. Frierson, and D. L. Hartmann, 2013: The relationship between the ITCZ and the Southern Hemispheric eddy-driven jet. *J. Geophys. Res. Atmos.*, **118**, 5136–5146, https://doi.org/10.1002/JGRD.50461.

Chemke, R., and L. M. Polvani, 2019: Exploiting the abrupt $4 \times CO_2$ scenario to elucidate tropical expansion mechanisms. *J. Climate*, **32**, 859–875, https://doi.org/10.1175/JCLI-D-18-0330.1.

Collins, W. J., and Coauthors, 2011: Development and evaluation of an Earth-system model—HadGEM2. *Geosci. Model Dev.*, **4**, 1051–1075, https://doi.org/10.5194/gmd-4-1051-2011.

Crutzen, P. J., 2006: Albedo enhancements by stratospheric sulfur injections: A contribution to resolve a policy dilemma? *Climatic Change*, **77**, 211–219, https://doi.org/10.1007/s10584-006-9101-y.

Cvijanovic, I., P. L. Langen, E. Kaas, and P. D. Ditlevsen, 2013: Southward intertropical convergence zone shifts and implications for an atmospheric bipolar seesaw. *J. Climate*, **26**, 4121–4137, https://doi.org/10.1175/JCLI-D-12-00279.1.

Delworth, T. L., and Coauthors, 2006: GFDL's CM2 global coupled climate models. Part I: Formulation and simulation characteristics. *J. Climate*, **19**, 643–674, https://doi.org/10.1175/JCLI3629.1.

Deser, C., R. A. Tomas, and L. Sun, 2015: The role of ocean–atmosphere coupling in the zonal-mean atmospheric response to Arctic sea ice loss. *J. Climate*, **28**, 2168–2186, https://doi.org/10.1175/JCLI-D-14-00325.1.

De Szoeke, S. P., and S. P. Xie, 2008: The tropical eastern Pacific seasonal cycle: Assessment of errors and mechanisms in IPCC AR4 coupled ocean–atmosphere general circulation models. *J. Climate*, **21**, 2573–2590, https://doi.org/10.1175/2007JCLI1975.1.

Dufresne, J.-L., and Coauthors, 2013: Climate change projections using the IPSL-CM5 Earth System Model: From CMIP3 to CMIP5. *Climate Dyn.*, **40**, 2123–2165, https://doi.org/10.1007/s00382-012-1636-1.

Dunstone, N., D. Smith, B. Booth, L. Hermanson, and R. Eade, 2013: Anthropogenic aerosol forcing of Atlantic tropical storms. *Nat. Geosci.*, **6**, 534–539, https://doi.org/10.1038/ngeo1854.

Forster, P. M., and Coauthors, 2016: Recommendations for diagnosing effective radiative forcing from climate models for CMIP6. *J. Geophys. Res. Atmos.*, **121**, 12 460–12 475, https://doi.org/10.1002/2016JD025320.

Frey, W. R., E. A. Maroon, A. G. Pendergrass, and J. E. Kay, 2017: Do Southern Ocean cloud feedbacks matter for 21st century warming? *Geophys. Res. Lett.*, **44**, 12 447–12 456, https://doi.org/10.1002/2017GL076339.

Green, B., and J. Marshall, 2017: Coupling of trade winds with ocean circulation damps ITCZ shifts. *J. Climate*, **30**, 4395–4411, https://doi.org/10.1175/JCLI-D-16-0818.1.

——, ——, and J.-M. Campin, 2019: The 'sticky' ITCZ: Ocean-moderated ITCZ shifts. *Climate Dyn.*, **53**, 1–19, https://doi.org/10.1007/s00382-019-04623-5.

Gregory, J. M., and Coauthors, 2004: A new method for diagnosing radiative forcing and climate sensitivity. *Geophys. Res. Lett.*, **31**, L03205, https://doi.org/10.1029/2003GL018747.

Hawcroft, M., J. M. Haywood, M. Collins, A. Jones, A. C. Jones, and G. Stephens, 2017: Southern Ocean albedo, inter-hemispheric energy transports and the double ITCZ: Global impacts of biases in a coupled model. *Climate Dyn.*, **48**, 2279–2295, https://doi.org/10.1007/s00382-016-3205-5.

——, ——, ——, and ——, 2018: The contrasting climate response to tropical and extratropical energy perturbations. *Climate Dyn.*, **51**, 3231–3249, https://doi.org/10.1007/S00382-018-4076-8.

Hirota, N., Y. N. Takayabu, M. Watanabe, and M. Kimoto, 2011: Precipitation reproducibility over tropical oceans and its relationship to the double ITCZ problem in CMIP3 and MIROC5 climate models. *J. Climate*, **24**, 4859–4873, https://doi.org/10.1175/2011JCLI4156.1.

Hoskins, B. J., and D. J. Karoly, 1981: The steady linear response of a spherical atmosphere to thermal and orographic forcing. *J. Atmos. Sci.*, **38**, 1179–1196, https://doi.org/10.1175/1520-0469(1981)038<1179:TSLROA>2.0.CO;2.

Hurrell, J. W., and Coauthors, 2013: The Community Earth System Model: A framework for collaborative research. *Bull. Amer. Meteor. Soc.*, **94**, 1339–1360, https://doi.org/10.1175/BAMS-D-12-00121.1.

Hwang, Y.-T., and D. M. Frierson, 2013: Link between the double-intertropical convergence zone problem and cloud biases over the Southern Ocean. *Proc. Natl. Acad. Sci. USA*, **110**, 4935–4940, https://doi.org/10.1073/pnas.1213302110.

Jones, A. C., J. M. Haywood, N. Dunstone, K. Emanuel, M. K. Hawcroft, K. I. Hodges, and A. Jones, 2017: Impacts of hemispheric solar geoengineering on tropical cyclone frequency. *Nat. Commun.*, **8**, 1382, https://doi.org/10.1038/s41467-017-01606-0.

Kang, S. M., and J. Lu, 2012: Expansion of the Hadley Cell under global warming: Winter versus summer. *J. Climate*, **25**, 8387–8393, https://doi.org/10.1175/JCLI-D-12-00323.1.

——, I. M. Held, D. M. Frierson, and M. Zhao, 2008: The response of the ITCZ to extratropical thermal forcing: Idealized slab-ocean experiments with a GCM. *J. Climate*, **21**, 3521–3532, https://doi.org/10.1175/2007JCLI2146.1.

——, D. M. Frierson, and I. M. Held, 2009: The tropical response to extratropical thermal forcing in an idealized GCM: The importance of radiative feedbacks and convective parameterization. *J. Atmos. Sci.*, **66**, 2812–2827, https://doi.org/10.1175/2009JAS2924.1.

——, Y. Shin, and S. P. Xie, 2018a: Extratropical forcing and tropical rainfall distribution: Energetics framework and ocean Ekman advection. *npj Climate Atmos. Sci.*, **1**, 20172, https://doi.org/10.1038/S41612-017-0004-6.

——, ——, and F. Codron, 2018b: The partitioning of poleward energy transport response between the atmosphere and Ekman flux to prescribed surface forcing in a simplified GCM. *Geosci. Lett.*, **5**, 22, https://doi.org/10.1186/s40562-018-0124-9.

Kay, J. E., C. Wall, V. Yettella, B. Medeiros, C. Hannay, P. Caldwell, and C. Bitz, 2016: Global climate impacts of fixing the Southern Ocean shortwave radiation bias in the Community Earth System Model (CESM). *J. Climate*, **29**, 4617–4636, https://doi.org/10.1175/JCLI-D-15-0358.1.

Kohyama, T., D. L. Hartmann, and D. S. Battisti, 2017: La Niña–like mean-state response to global warming and potential oceanic roles. *J. Climate*, **30**, 4207–4225, https://doi.org/10.1175/JCLI-D-16-0441.1.

Li, C., L. Wu, and S.-P. Xie, 2013: Impacts of interhemispheric asymmetric thermal forcing on tropical Pacific climate: Surface air–sea coupling and subduction. *J. Climate*, **26**, 575–582, https://doi.org/10.1175/JCLI-D-11-00743.1.

Li, G., and S. P. Xie, 2014: Tropical biases in CMIP5 multimodel ensemble: The excessive equatorial Pacific cold tongue and double ITCZ problems. *J. Climate*, **27**, 1765–1780, https://doi.org/10.1175/JCLI-D-13-00337.1.

Lin, J.-L., 2007: The double-ITCZ problem in IPCC AR4 coupled GCMs: Ocean–atmosphere feedback analysis. *J. Climate*, **20**, 4497–4525, https://doi.org/10.1175/JCLI4272.1.

Liu, F., J. Lu, O. Garuba, L. R. Leung, Y. Luo, and X. Wan, 2018: Sensitivity of surface temperature to oceanic forcing via *q*-flux Green's function experiments. Part I: Linear response function. *J. Climate*, **31**, 3625–3641, https://doi.org/10.1175/JCLI-D-17-0462.1.

Liu, W., J. Lu, S.-P. Xie, and A. Fedorov, 2018: Southern Ocean heat uptake, redistribution, and storage in a warming climate: The role of meridional overturning circulation. *J. Climate*, **31**, 4727–4743, https://doi.org/10.1175/JCLI-D-17-0761.1.

Ma, C.-C., C. R. Mechoso, A. W. Robertson, and A. Arakawa, 1996: Peruvian stratus clouds and the tropical Pacific circulation: A coupled ocean–atmosphere GCM study. *J. Climate*, **9**, 1635–1645, https://doi.org/10.1175/1520-0442(1996)009<1635:PSCATT>2.0.CO;2.

Martin, G. M., and Coauthors, 2011: The HadGEM2 family of Met Office Unified Model climate configurations. *Geosci. Model Dev.*, **4**, 723–757, https://doi.org/10.5194/gmd-4-723-2011.

Mauritsen, T., and Coauthors, 2019: Developments in the MPI-M Earth System Model version 1.2 (MPI-ESM1.2) and its response to increasing CO_2. *J. Adv. Model. Earth Syst.*, **11**, 998–1038, https://doi.org/10.1029/2018MS001400.

Mechoso, C. R., and Coauthors, 1995: The seasonal cycle over the tropical Pacific in coupled ocean–atmosphere general circulation models. *Mon. Wea. Rev.*, **123**, 2825–2838, https://doi.org/10.1175/1520-0493(1995)123<2825:TSCOTT>2.0.CO;2.

——, and Coauthors, 2016: Can reducing the incoming energy flux over the Southern Ocean in a CGCM improve its simulation of tropical climate? *Geophys. Res. Lett.*, **43**, 11 057–11 063, https://doi.org/10.1002/2016GL071150.

Merlis, T. M., M. Zhao, and I. M. Held, 2013: The sensitivity of hurricane frequency to ITCZ changes and radiatively forced warming in aquaplanet simulations. *Geophys. Res. Lett.*, **40**, 4109–4114, https://doi.org/10.1002/grl.50680.

Mitchell, D., and Coauthors, 2017: Half a degree Additional warming, Projections, Prognosis and Impacts (HAPPI): Background and experimental design. *Geosci. Model Dev.*, **10**, 571–583, https://doi.org/10.5194/gmd-10-571-2017.

Müller, W. A., and Coauthors, 2018: A high-resolution version of the Max Planck Institute Earth System Model (MPI-ESM1.2-HR). *J. Adv. Model. Earth Syst.*, **10**, 1383–1413, https://doi.org/10.1029/2017MS001217.

Myhre, G., and Coauthors, 2013: Anthropogenic and natural radiative forcing. *Climate Change 2013: The Physical Science Basis*, T. F. Stocker et al., Eds., Cambridge University Press, 659–740.

Pendergrass, A. G., A. Conley, and F. M. Vitt, 2018: Surface and top-of-atmosphere radiative feedback kernels for CESM-CAM5. *Earth Syst. Sci. Data*, **10**, 317–324, https://doi.org/10.5194/essd-10-317-2018.

Schneider, T., 2017: Feedback of atmosphere-ocean coupling on shifts of the intertropical convergence zone. *Geophys. Res. Lett.*, **44**, 11 644–11 653, https://doi.org/10.1002/2017GL075817.

Screen, J. A., and Coauthors, 2018: Consistency and causes of discrepancy in the atmospheric response

to Arctic sea ice loss across climate models. *Nat. Geosci.*, **11**, 155–163, https://doi.org/10.1038/S41561-018-0059-Y.

Seo, J., S. M. Kang, and D. M. W. Frierson, 2014: Sensitivity of intertropical convergence zone movement to the latitudinal position of thermal forcing. *J. Climate*, **27**, 3035–3042, https://doi.org/10.1175/JCLI-D-13-00691.1.

Serreze, M. C., and R. G. Barry, 2011: Processes and impacts of Arctic amplification: A research synthesis. *Global Planet. Change*, **77**, 85–96, https://doi.org/10.1016/j.gloplacha.2011.03.004.

Sherwood, S. C., S. Bony, O. Boucher, C. Bretherton, P. M. Forster, J. M. Gregory, and B. Stevens, 2015: Adjustments in the forcing–feedback framework for understanding climate change. *Bull. Amer. Meteor. Soc.*, **96**, 217–228, https://doi.org/10.1175/BAMS-D-13-00167.1.

Song, X., and G. J. Zhang, 2018: The roles of convection parameterization in the formation of double ITCZ syndrome in the NCAR CESM: I. Atmospheric processes. *J. Adv. Model. Earth Syst.*, **10**, 842–866, https://doi.org/10.1002/2017MS001191.

Stuecker, M. F., and Coauthors, 2018: Polar amplification dominated by local forcing and feedbacks. *Nat. Climate Change*, **8**, 1076–1081, https://doi.org/10.1038/s41558-018-0339-y.

Taylor, K., and Coauthors, 2007: Estimating shortwave radiative forcing and response in climate models. *J. Climate*, **20**, 2530–2543, https://doi.org/10.1175/JCLI4143.1.

Timmermann, A., and Coauthors, 2007: The influence of a weakening of the Atlantic meridional overturning circulation on ENSO. *J. Climate*, **20**, 4899–4919, https://doi.org/10.1175/JCLI4283.1.

Voigt, A., B. Stevens, J. Bader, and T. Mauritsen, 2013: The observed hemispheric symmetry in reflected shortwave irradiance. *J. Climate*, **26**, 468–477, https://doi.org/10.1175/JCLI-D-12-00132.1.

Wang, K., C. Deser, L. Sun, and R. A. Tomas, 2018: Fast response of the tropics to an abrupt loss of Arctic sea ice via ocean dynamics. *Geophys. Res. Lett.*, **45**, 4264–4272, https://doi.org/10.1029/2018GL077325.

Watanabe, M., H. Shiogama, H. Tatebe, M. Hayashi, M. Ishii, and M. Kimoto, 2014: Contribution of natural decadal variability to global-warming acceleration and hiatus. *Nat. Climate Change*, **4**, 893–897, https://doi.org/10.1038/nclimate2355.

White, R. H., A. A. McFarlane, D. M. W. Frierson, S. M. Kang, Y. Shin, and M. Friedman, 2018: Tropical precipitation and cross-equatorial heat transport in response to localized heating: Basin and hemisphere dependence. *Geophys. Res. Lett.*, **45**, 11 949–11 958, https://doi.org/10.1029/2018GL078781.

Wood, R., and C. S. Bretherton, 2006: On the relationship between stratiform low cloud cover and lower-tropospheric stability. *J. Climate*, **19**, 6425–6432, https://doi.org/10.1175/JCLI3988.1.

Xiang, B., M. Zhao, I. M. Held, and J.-C. Golaz, 2017: Predicting the severity of spurious "double ITCZ" problem in CMIP5 coupled models from AMIP simulations. *Geophys. Res. Lett.*, **44**, 1520–1527, https://doi.org/10.1002/2016GL071992.

——, ——, Y. Ming, W. Yu, and S. M. Kang, 2018: Contrasting impacts of radiative forcing in the Southern Ocean versus southern tropics on ITCZ position and energy transport in one GFDL climate model. *J. Climate*, **31**, 5609–5628, https://doi.org/10.1175/JCLI-D-17-0566.1.

Yu, S., and M. Pritchard, 2019: A strong role for the AMOC in partitioning global energy transport and shifting ITCZ position in response to latitudinally discrete solar forcing in the CESM1.2. *J. Climate*, **32**, 2207–2226, https://doi.org/10.1175/JCLI-D-18-0360.1.

Zhang, X. X., H. L. Liu, and M. H. Zhang, 2015: Double ITCZ in coupled ocean-atmosphere models: From CMIP3 to CMIP5. *Geophys. Res. Lett.*, **42**, 8651–8659, https://doi.org/10.1002/2015GL065973.

Zhao, M., and Coauthors, 2018: The GFDL global atmosphere and land model AM4.0/LM4.0: 1. Simulation characteristic with prescribed SSTs. *J. Adv. Model. Earth Syst.*, **10**, 691–734, https://doi.org/10.1002/2017MS001208.

Zheng, Y. X., T. Shinoda, J. L. Lin, and G. N. Kiladis, 2011: Sea surface temperature biases under the stratus cloud deck in the southeast Pacific Ocean in 19 IPCC AR4 coupled general circulation models. *J. Climate*, **24**, 4139–4164, https://doi.org/10.1175/2011JCLI4172.1.

Zhou, C., M. D. Zelinka, and S. A. Klein, 2017: Analyzing the dependence of global cloud feedback on the spatial pattern of sea surface temperature change with a Green's function approach: Analyzing cloud feedback with GFA. *J. Adv. Model. Earth Syst.*, **9**, 2174–2189, https://doi.org/10.1002/2017MS001096.

Zhou, Z.-Q., and S.-P. Xie, 2015: Effects of climatological model biases on the projection of tropical climate change. *J. Climate*, **28**, 9909–9917, https://doi.org/10.1175/JCLI-D-15-0243.1.